Available online at www.sciencedirect.com
ScienceDirect
Acta Biomaterialia 5 (2009) 1082–1093
Acta BIOMATERIALIA
www.elsevier.com/locate/actabiomat

Engineered μ-bimodal poly(ε-caprolactone) porous scaffold for enhanced hMSC colonization and proliferation

A. Salerno [a,b], D. Guarnieri [a], M. Iannone [a,c], S. Zeppetelli [d], E. Di Maio [c], S. Iannace [d], P.A. Netti [a,b,*]

[a] *Interdisciplinary Research Centre on Biomaterials, CRIB, University of Naples Federico II, Piazzale Tecchio 80, 80125 Naples, Italy*
[b] *Italian Institute of Technology, IIT, University of Naples Federico II, Piazzale Tecchio 80, 80125 Naples, Italy*
[c] *Department of Materials and Production Engineering, DIMP, University of Naples Federico II, University of Naples Federico II, Piazzale Tecchio 80, 80125 Naples, Italy*
[d] *Institute of Composite and Biomedical Materials and National Research Council, IMCB-CNR, University of Naples Federico II, Piazzale Tecchio 80, 80125 Naples, Italy*

Received 7 July 2008; received in revised form 8 October 2008; accepted 20 October 2008
Available online 5 November 2008

Abstract

The use of scaffold-based strategies in the regeneration of biological tissues requires that the design of the microarchitecture of the scaffold satisfy key microstructural and biological requirements. Here, we examined the ability of a porous poly(ε-caprolactone) (PCL) scaffold with novel bimodal-micron scale (μ-bimodal) porous architecture to promote and guide the in vitro adhesion, proliferation and three-dimensional (3-D) colonization of human mesenchymal stem cells (hMSCs). The μ-bimodal PCL scaffold was prepared by a combination of gas foaming (GF) and selective polymer extraction (PE) from co-continuous blends. The microarchitectural properties of the scaffold, in particular its morphology, porosity distribution and mechanical compression properties, were analyzed and correlated with the results of the in vitro cell–scaffold interaction study, carried out for 21 days under static conditions. Alamar Blue assay, scanning electron microscopy, confocal laser scanning microscopy and histological analyses were performed to assess hMSC adhesion, proliferation and 3-D colonization. The results showed that the combined GF–PE technique allowed the preparation of PCL scaffold with a unique multiscaled and highly interconnected microarchitecture that was characterized by mechanical properties suitable for load-bearing applications. Study of the cell–scaffold interaction also demonstrated the ability of the scaffold to support hMSC adhesion and proliferation, as well as the possibility to promote and guide 3-D cell colonization by appropriately designing the microarchitectural features of the scaffold.

Keywords: Gas foaming; Microstructure; Poly(ε-caprolactone); Scaffold; Stem cell

1. Introduction

Tissue engineering aims at the repair of damaged biological tissues circumventing the limitations of the traditional medical approaches, such as transplantation, by using a combination of material, cells and molecular cues [1,2]. One of the most important challenges in tissue engineering is the appropriate design of open-pore biocompatible and biodegradable porous scaffolds that are able to provide a temporary substitute for the extracellular matrix. The scaffold must promote cell adhesion, proliferation and biosynthesis, must allow fluid transport, and must sustain the external mechanical stress until the regeneration of the functional new tissue is completed [3–5].

Although not all the details of scaffold design requirements have been completely defined, a large number of studies have explored the effects of the topographical features of the scaffold on cellular responses [6–9]. These studies demonstrated that the microarchitecture of the scaffold

* Corresponding author. Address: Interdisciplinary Research Centre on Biomaterials, CRIB, University of Naples Federico II, Piazzale Tecchio 80, 80125 Naples, Italy. Tel.: +39 081 7682408; fax: +39 081 7682404.
E-mail address: nettipa@unina.it (P.A. Netti).

1742-7061/$ - see front matter © 2008 Acta Materialia Inc. Published by Elsevier Ltd. All rights reserved.
doi:10.1016/j.actbio.2008.10.012

may guide cell functions by regulating the interaction between cells, and the diffusion of nutrients and metabolic wastes throughout the three-dimensional (3-D) construct [6–9]. In particular, the scaffold-assisted regeneration of specific tissues has been shown to be strongly dependent on the scaffold's surface-to-volume ratio and pore size and interconnectivity. Indeed, these microarchitectural features significantly influence cell morphology, cell binding and phenotypic expression, but also control the extent and nature of nutrient diffusion and tissue ingrowth [6–9].

Furthermore, it has been suggested that the pore dimensions may directly affect some biological events and, as a result, different tissues require optimal pore sizes for their regeneration [6–8]. Therefore, scaffolds with bimodal-micron scale (μ-bimodal) porosities may be often necessary for the regeneration of highly structured biological tissues, such as bone and cartilage [7].

On the other hand, transport issues, 3-D cell colonization and tissue ingrowth would be inhibited if the pores are not well interconnected, even if the porosity of the scaffolds is high [9].

For the success of any tissue engineering scaffold-based strategy, the issue of the mechanical function is essential, and is one of the critical aspects in scaffold design. Indeed, there is often a conflict between maximizing surface-to-volume ratio to enhance cell colonization and fluid transport, and optimizing the mechanical response of the scaffold. This conflict often leads to a compromise in the optimal design solution [10].

To date, many different strategies have been developed to overcome the transport limitations and the lack of tissue infiltration into the interior of the scaffold, without affecting its mechanical function.

The use of dynamic cell seeding and cultivation devices, in particular perfusion bioreactors or spinner flasks, results in increased proliferation, differentiation and distribution of cells into the scaffold [11–14]. Nevertheless, without an appropriate scaffold microarchitecture, this solution may be unsuitable to ensure the ingrowth of new tissue and to prevent the development of a necrotic core caused by diffusion constraints into the interior of the construct.

In this study, a new approach in the design of μ-bimodal porous scaffold is presented, and the microstructural properties and biocompatibility of the obtained scaffold evaluated. Poly(ε-caprolactone) (PCL) was selected for the preparation of the scaffold because of its proved biocompatibility [15–17] and processability properties [18]. As previously reported [19], the PCL scaffold was prepared by the combination of gas foaming (GF) and selective polymer extraction (PE) from co-continuous blends. In particular, the μ-bimodal porous architecture of the scaffold was designed with a strait porosity of the order of hundreds of microns (macroporosity), for rapid cell colonization and tissue ingrowth, with a built-in one order of magnitude lower porosity (microporosity), that may serve as preferential route for fluid transport.

The microstructural features and the mechanical function of the scaffold were evaluated by scanning electron microscopy (SEM), porosity distribution analysis and static compression testing. Furthermore, the cell–scaffold interaction was studied using human mesenchymal stem cells (hMSCs) in vitro culture, for 21 days and under static conditions. Alamar Blue assay was performed to evaluate cell proliferation, while cell adhesion and 3-D colonization were assessed by SEM, confocal laser scanning microscopy (CLSM) and histological analyses. Finally, the results of the cell–scaffold interaction study were compared with those obtained by seeding hMSCs into PCL scaffolds with monomodal porosity distribution in order to address whether different scaffold microarchitectures may govern cell adhesion and spatial distribution in 3-D porous structures.

2. Materials and methods

2.1. Scaffold fabrication

As schematically illustrated in Fig. 1, the GF–PE technique is characterized by three different steps [19]: (1) 3/2 (w/w) PCL/thermoplastic gelatin (TG) co-continuous blend was prepared by melt mixing in an internal mixer (Rheomix® 600 Haake, Germany) at 60 °C and 80 rpm for 6 min (Fig. 1A); (2) the PCL/TG blend was subsequently gas foamed with a 4/1 (v/v) N_2/CO_2 blowing mixture, at a foaming temperature (T_F) of 44 °C and with a pressure drop rate (PDR) of 700 bar s^{-1} (Fig. 1B); (3) finally, the TG was selectively extracted from the foamed blend by soaking the sample in dH_2O (Fig. 1C).

2.2. Microstructural characterization

2.2.1. Morphology and porosity

The microstructure of the scaffold was analyzed by SEM (S440, Leica, Germany). The scaffold was cross-sectioned, gold sputtered and analyzed at an accelerating voltage of 20 kV.

The overall porosity was determined from the mass and the volume of the scaffold by using the following equation [20]:

$$\%\ \text{porosity} = [1 - (\rho S/\rho_{PCL})] \times 100, \quad (1)$$

where ρ_S is the apparent density of the scaffold calculated from mass and volume measurements. The mass was measured by using a high accuracy balance (10^{-3} g, AB104-S, Mettler Toledo, Italy), while the volume was determined by geometrical calculation. The overall porosity data represents the mean value of five different porosity measurements.

Image analysis (Image J®) was used to assess the volume fraction of the two different scaled porosities by means of area fraction measurements [21,22]. In particular, the area fraction of the TG foamed phase provided the macroporosity volume fraction, while the difference between the mean overall porosity and the macroporosity amount yielded the

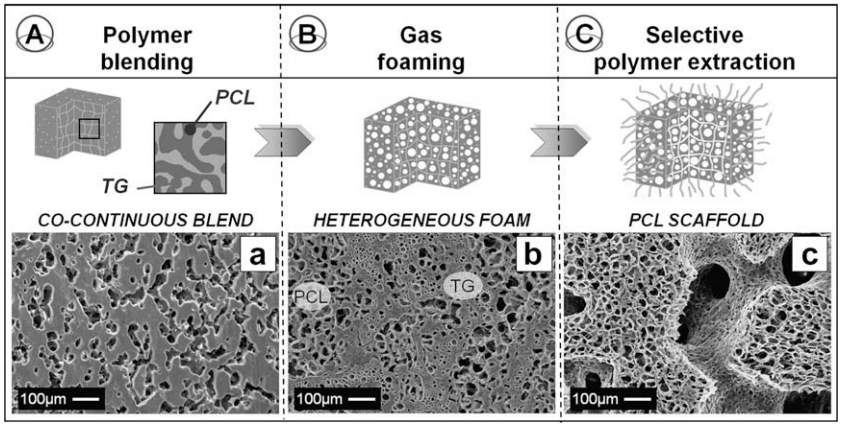

Fig. 1. Correspondence between the processing step and the microstructural evolution of PCL/TG system: (a) SEM micrograph of 3/2 (w/w) PCL/TG co-continuous blend after the selective extraction of the TG; (b) SEM micrograph of PCL/TG blend foamed with 4/1 (v/v) N_2/CO_2 blowing mixture, at $T_F = 44$°C and PDR = 700 bar/s; (c) SEM micrograph of μ-bimodal PCL scaffold prepared by the selective extraction of the TG from the foamed PCL/TG blend.

microporosity volume fraction. Image analysis was also used to evaluate the mean pore size of the microporosity, based on the ASTM D3576 method.

2.2.2. Mechanical properties

Static compression testing was used to evaluate the mechanical response of the PCL scaffold. Five disc-shaped scaffolds (d = 10 mm and h = 3 mm) were tested on an Instron machine (4204, Instron, Italy) at a cross head of 1 mm min^{-1} and with a 1 kN loading cell. The elastic compression modulus was determined as the slope of the initial linear portion of the stress vs. strain curve, while the compression yield strength was calculated with the modulus slope at an offset of 1% strain.

2.3. hMSC expansion, seeding and culture

Bone-marrow-derived hMSCs (Clonetics, Italy), at the 7th passage, were cultured in α-Modified Eagle's medium (α-MEM) (Bio Wittaker, Belgium) containing 10% (v/v) FBS, 100 U ml^{-1} penicillin and 0.1 mg ml^{-1} streptomycin (HyClone, UK), in a humidified atmosphere at 37 °C and 5% CO_2.

Scaffolds for cell-culture experiments (d = 10 mm and h = 3 mm) were γ-sterilized before seeding. 4×10^5 cells $scaffold^{-1}$, resuspended in 50 μl of medium, were statically seeded onto the scaffold. Following seeding, the scaffolds were placed in 24 well culture plates (1 scaffold $well^{-1}$) and, incubated for 2 h in a humidified atmosphere (37 °C, 5% CO_2). Subsequently, 1.5 ml of cell-culture medium was added to each well. The scaffolds were maintained in culture for 21 days and the cell-culture medium was changed every 3–4 days.

2.4. Cell–scaffold interaction study

2.4.1. Alamar Blue assay

Cell viability and proliferation were evaluated by using the Alamar Blue assay. The cell–scaffold constructs were removed from the culture plates at days 1, 7, 14 and 21, washed with PBS (Sigma–Aldrich, Italy), and placed into 24 well culture plates. For each construct, 2 ml of DMEM medium without Phenol Red (HyClone, UK) containing 10% (v/v) Alamar Blue (AbD Serotec Ltd, UK) were added, followed by incubation for 4 h at 37 °C and 5% CO_2. The solution was subsequently removed from the wells and analyzed by a spectrophotometer (multilabel counter, 1420 Victor, Perkin Elmer, Italy) at wavelengths of 570 and 600 nm. The number of viable cells into the scaffolds was finally determined by comparing the absorbance values at different culture times with those of the calibration curve. The calibration curve was obtained from the correlation between known cell numbers in the 24 well culture plates with the corresponding absorbance values.

2.4.2. SEM

SEM analysis was performed to evaluate cell morphology and colonization at 7, 14 and 21 days after seeding. The cell–scaffold constructs were extracted from the wells, washed with PBS and fixed with 2.5% glutaraldehyde (Sigma–Aldrich, Italy) in 0.1 M Na-cacodylate (Carlo Erba, Italy) at pH 7.4. Before examination, the constructs were dehydrated in graded ethanol concentrations (from 50% to 100% v/v in ethanol), air-dried and sputter-coated with gold. To evaluate hMSC morphology and colonization into the inner part of the scaffold, the constructs were embedded under vacuum with Compound Tissue Tek (OCT, Bio-Optica, Italy) and cryogenically sectioned, transverse to the seeding surface, as described in Ref. [17]. The samples were subsequently gold sputtered and analyzed by SEM. As negative controls, PCL scaffolds without cells were analyzed by following the same protocol.

2.4.3. CLSM

For CLSM analysis, the constructs were extracted from the wells at 1, 7, 14 and 21 days after seeding, fixed with 4% paraphormaldeyde for 20 min at RT, rinsed twice with PBS

buffer and incubated with PBS–BSA 0.5% to block nonspecific binding. Actin microfilaments were stained with phalloidin tetramethylrhodamine B isothiocyanate (Sigma–Aldrich, Italy). Phalloidin was diluted in PBS–BSA 0.5% and incubated for 30 min at RT. Nucleus detection was performed by using 4′,6-diamidino-2-phenylindole (DAPI) (Sigma–Aldrich, Italy). DAPI stock solution (10 mg ml^{-1} in DMSO) was diluted in PBS ($1/10^4$ v/v) and incubated for 10 min at 37 °C. To evaluate hMSC colonization in 3-D, the DAPI staining was also performed on 100 μm cryosections, transverse to the seeding surface, obtained as previously described. Samples were then rinsed three times with PBS and observed by an inverted fluorescence microscope (IX50, Olympus, Italy), using 4×, 10× and 20× objectives.

2.4.4. Histology

The effect of the microarchitecture of the scaffold on hMSC morphology and 3-D colonization was additionally surveyed by histological analysis. 50 μm cryostat sections, transverse to the seeding surface, were stained with hematoxylin–eosin (H–E) following standard procedures.

2.4.5. Statistical analysis

Data are presented as mean ± standard deviation. The statistical significance of the Alamar Blue results was assessed by one-way ANOVA at the significance level $P < 0.05$, using Origin® software.

3. Results

3.1. Microstructural properties of the scaffold

The schematic steps of the process to achieve the μ-bimodal porous scaffold are reported in Fig. 1 along with typical SEM micrographs of a specimen's cross-section. The process starts from the preparation of a co-continuous blend of PCL and TG, with a PCL weight fraction of 60%. After the extraction of the TG from the PCL/TG blend, the co-continuity of the gelatin phase was evident from the SEM micrograph of the cross-section of the specimen (Fig. 1a). Following the GF process, due to the incompatibility of the PCL/TG blend and to the different foaming behaviour of the two polymers [19], the microstructure of the PCL/TG foam was characterized by two different porous phases, with the PCL foamed phase characterized by a 40 μm mean pore size and a high degree of pore interconnection (Fig. 1b). The final removal of the TG from the foamed blend (Fig. 1c) allowed the formation of an additional porosity, characterized by elongated and highly interconnected macroporosity, passing through the rounded and smaller microporosity induced by the GF step.

Table 1 reports the porosity and mechanical compression properties data of the μ-bimodal PCL scaffold. It can be observed that the low concentration of TG templating (40 wt.%) and the optimization of the GF process

Table 1
Porosity and mechanical compression properties of the μ-bimodal PCL scaffold prepared. (a) SEM of the cross-section of the scaffold and (b) equivalent binary image used for the evaluation of the macroporosity volume fraction.

Overall porosity (%)	Macroporosity (%)		Macroporosity (%)	Compression modulus (MPa)	Compression yield strength (MPa)
62 ± 1.1	44	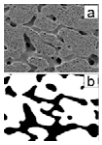	56	11.4 ± 1.2	1.6 ± 0.3

parameters allowed the preparation of PCL scaffold characterized by 62% mean overall porosity. Moreover, the image analysis also confirmed the low overall porosity level of the scaffold (pore volume equal to 64.1%) and showed that the porosity is uniformly distributed between the macroporosity created by the selective extraction of the TG and the microporosity, characterized by 40 μm mean pore size, induced by the GF process.

The results of the mechanical characterization showed the typical stress–strain curve of porous materials undergoing static compression testing (data not shown). In particular, the initial linear-elastic region was followed by a short collapse plateau and, finally, the steep increase in the stress values caused by the densification phenomenon was observed [23]. As reported in Table 1, the calculated average compression modulus and yield strength were 11.4 and 1.6 MPa, respectively.

3.2. Cell–scaffold interaction study

The Alamar Blue assay provided a quantitative evaluation of the number of viable cells in the scaffold [24]. The results of this test, reported in Fig. 2, are the average ± standard deviation of five samples, and show the cell

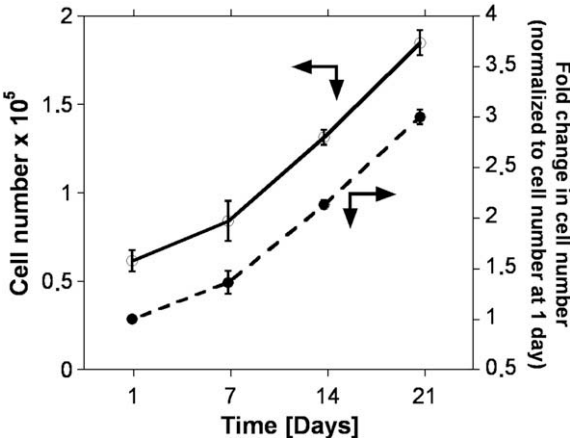

Fig. 2. hMSCs proliferation during 21 days of culture, measured by Alamar Blue assay: (○) cell number; (●) proliferation index.

proliferation over the culture time. In particular, during the in vitro static culture, the number of hMSCs increases from 6.2×10^4 at day 1 to 1.8×10^5 at day 21. There was a statistically significant difference ($P < 0.05$) in the cell number over the culture period. It is important to note that the seeding efficiency, evaluated by the difference between the number of cells in the seeding suspension and the number of cells in the culture plate after seeding, was about 80%.

Fig. 3a–g are SEM images of the seeding surfaces and cross-sections of the cell–scaffold constructs, at different culture times, showing cell morphology and colonization into the porous network of the scaffold. At 7 days of in vitro culture, hMSCs colonized the surface of the scaffold (Fig. 3a), adhering into the macroporosity (Fig. 3b, black arrow), and, additionally, the cells created bridges between the opposite pore walls (Fig. 3c). By increasing the culture time to 14 and 21 days, the presence of an uniform cell sheet on the scaffold surface was observed, and it was difficult to distinguish the supporting scaffold microarchitecture (Fig. 3d–f). In Fig. 3g is reported the SEM micrograph of the interior of the construct, at 21 days from seeding. This image, representative of a general trend, demonstrates that the cells colonized the inner macroporosity of the scaffold, adhering to the pore walls by multifocal points.

Actin cytoskeleton and nucleus staining was carried out to assess hMSC shape and distribution on and into the scaffold. As reported in Fig. 4a and c, 1 day after seeding, cells adhered to scaffold surface and appeared quite homogeneously distributed. By increasing cell-culture time, the number of the cells increased. As a direct consequence, at day 21, cells formed a dense layer and covered all the available surfaces of the scaffold (Fig. 4b and d). The higher magnifications reported in Fig. 4e and f also evidenced that, at 21 days of culture, the hMSC morphology is elongated and oriented, suggesting that they are becoming confluent.

Cross-sectional observations also indicated that cells were present within the scaffold already at 1 day from seeding, preferentially invading the macroporosity (Fig. 5). Moreover, the cells in the interior of the construct remained viable over the culture time, as observed by analyzing their nucleus shape (Fig. 5e and f).

Representative images of the histological sections of the constructs at different culture times are reported in Fig. 6. In agreement with the SEM and fluorescence microscopy data (Figs. 3 – 5), extensive colonization of the scaffold

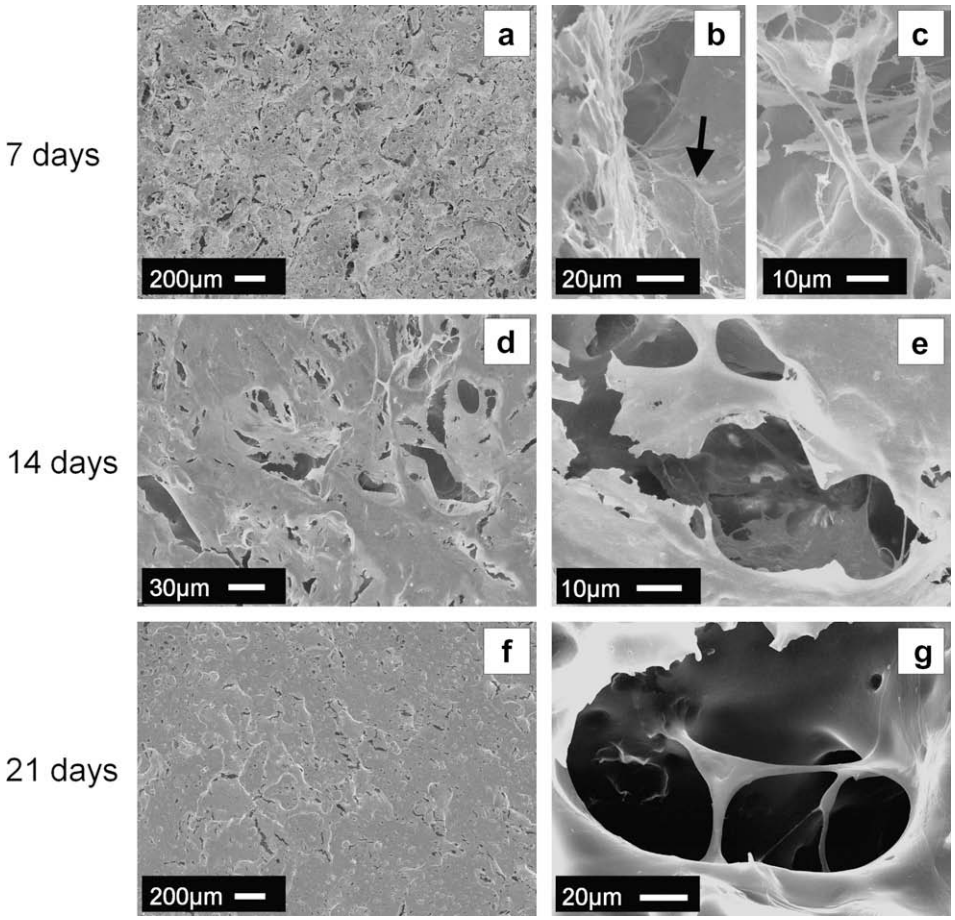

Fig. 3. SEM micrographs of the cell-scaffold constructs at different culture time: (a-f) cell seeding surfaces at 7 (a-c), 14 (d, e) and 21 (f) days of culture; transverse section of the 21 days cell-scaffold construct (g) showing representative hMSCs morphology into the macroporosity.

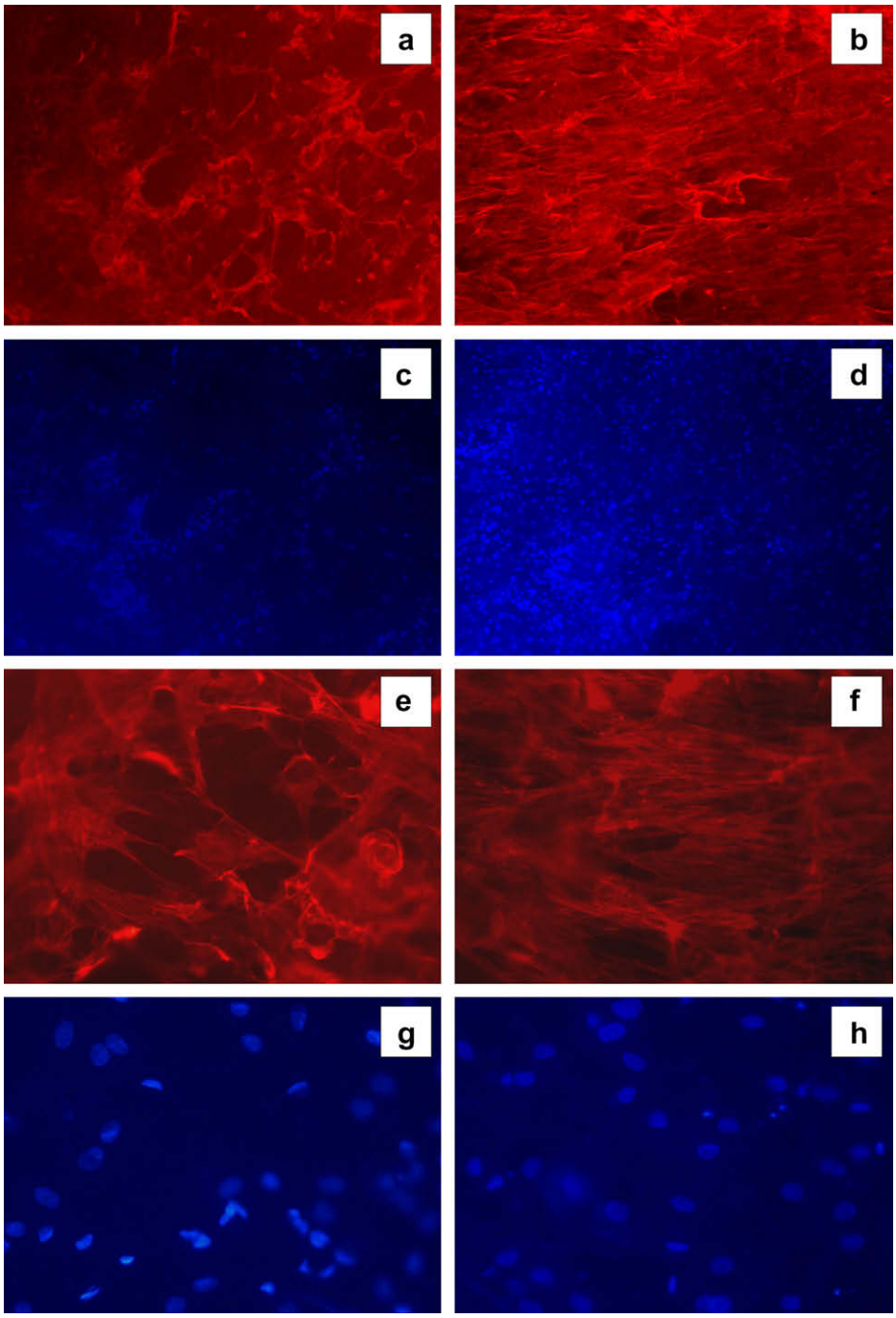

Fig. 4. Fluorescence microscope images of the surfaces of the cell-scaffold constructs showing actin cytoskeleton stained by phalloidin and cell nuclei stained by DAPI, at 1 day (left column) and 21 days (right column) of culture. Figures a-d (objective 4x), figures e-h (objective 20x).

by the hMSCs was observed, into the outer and inner surfaces. Moreover, the histochemical analysis may allow a more detailed evaluation of the morphology and distribution of the cells into the microarchitecture of the scaffold.

At 7 days of cell-culture, Fig. 6a and b, we observed that the colonization does not occur uniformly throughout the 3-D architecture, but the cells rather preferentially colonized the macroporosity of the scaffold. This effect may be related to the ability of the macroporosity architecture to promote the diffusion of the cell-culture medium into the inner region of the scaffold, during cell seeding (see also the cross-sections reported in Fig. 5). By increasing the culture time up to 14 and 21 days (Fig. 6c–f), the enhanced cell proliferation and colonization both on the surface (Fig. 6c) and into the interior of the construct (Fig. 6d–f) could clearly be seen. Furthermore, in agreement with the results of the SEM analysis reported in Fig. 3g, the cells in the macroporosity stretched, creating bridges between the opposite pore walls (lower and higher magnification reported in Fig. 6e and f).

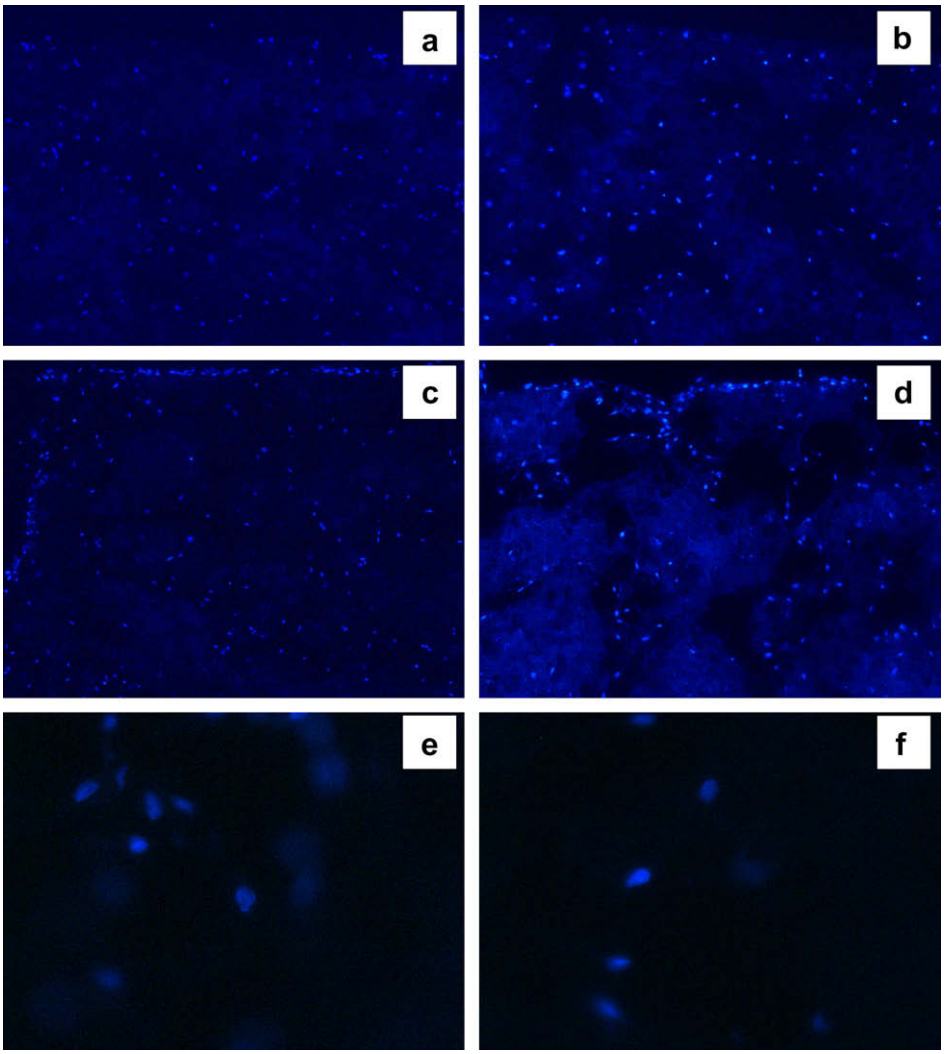

Fig. 5. Fluorescence microscope images of the cross sections of the cell-scaffold constructs showing cell nuclei stained by DAPI: (a, e) 1 day; (b) 7 days; (c) 14 days and (d, f) 21 days. Figures a-d (objective 4x), figures e and f (objective 20x).

Additional hMSC culture was performed on PCL scaffolds with a monomodal porosity distribution, in order to assess whether the topological properties of the porous structure of the scaffold may govern cell adhesion and 3-D spatial distribution. Fig. 7 shows the SEM micrograph and the pore size distribution of PCL scaffold prepared by using the GF/PE combined technology and by performing foaming at $T_F = 70$ °C. As can be seen in Fig. 7a, when the foaming process was carried out at temperatures higher than the PCL melting temperature, the final scaffold microarchitecture was characterized by a monomodal porosity distribution. In particular, these scaffolds exhibited an overall porosity of 61% and a mean pore size of 325 ± 190 μm (see Fig. 7b).

Representative fluorescence and histological images of the cross-sections of the cell–scaffold constructs at day 1 after seeding are reported in Fig. 8. Fig. 8a and b show that the monomodal PCL scaffolds were able to support hMSC adhesion and 3-D colonization. However, a nonuniform cell distribution was achieved between the surface and the inner region of the scaffold. Indeed, it was possible to observe large clusters of cells on the scaffold surface, as well as the progressive reduction of hMSC colonization in the inner region of the porous structure (see Fig. 8a and b). These results were also confirmed by the analysis of the histological images of the cross-sections of the cell–scaffold construct, reported in Fig. 8c and d. In particular, nonuniform hMSC distribution was observed on the surface of the scaffold (black arrows), and heterogeneous cell colonization was achieved between the outer and inner region of the porous structure.

4. Discussion

Scaffold design is becoming essential for the success of any scaffold-based tissue engineering strategies. Cell guidance by the scaffold, from cell-material construct to the new engineered tissue, requires a complex balance between chemical, biochemical and biophysical cues able to mimic the spatial and temporal microenvironments of the natural

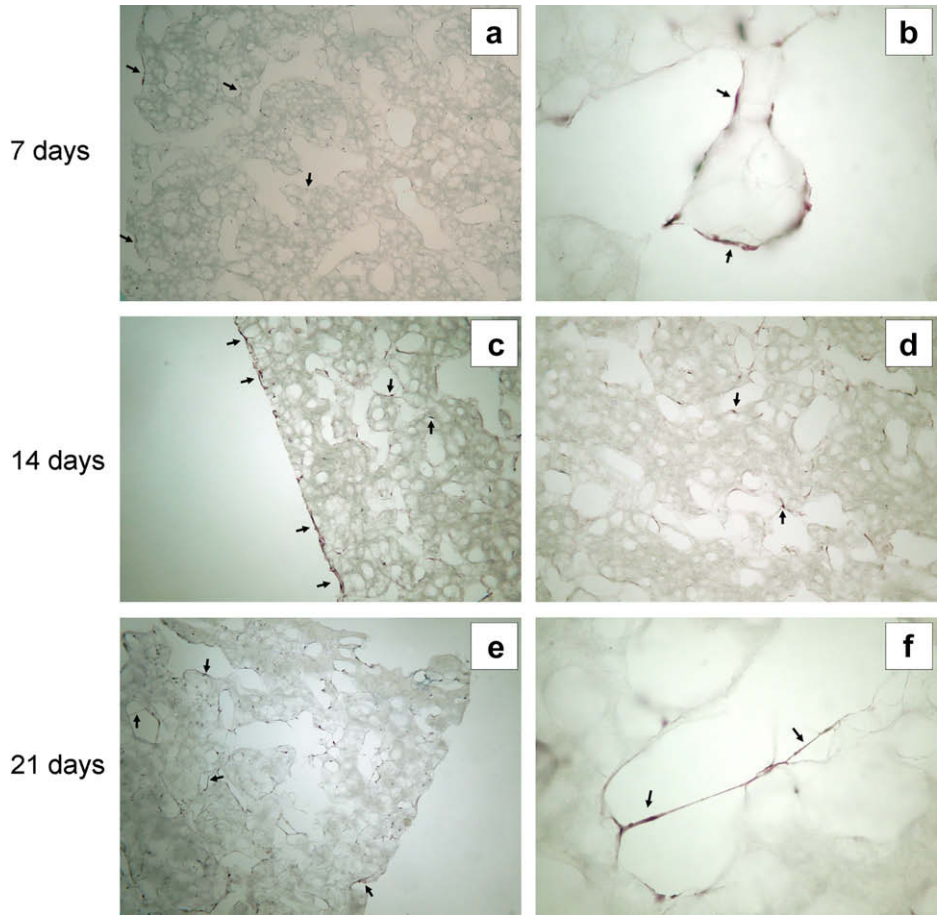

Fig. 6. Representative light images of transverse sections of the cell-scaffold constructs, stained with H & E at 7 (a,b), 14 (c,d)and 21 (e,f) days of culture. The black arrows indicated some representative hMSCs into different regions of the scaffold.

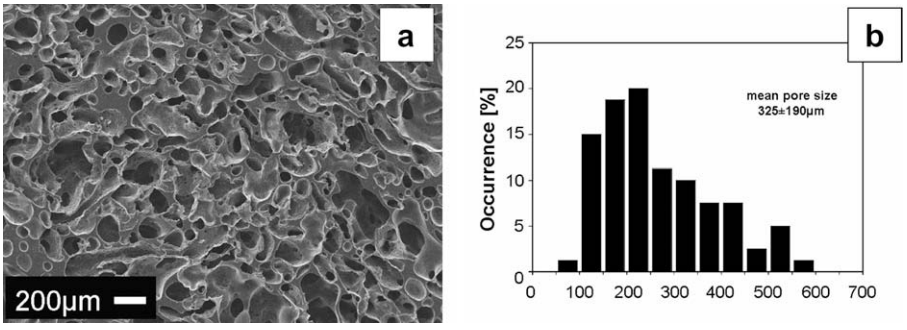

Fig. 7. (a) SEM micrograph and (b) pore size distribution of PCL scaffold with monomodals porosity distribution obtained by the GF/PE combined technology and performing the foaming process at $T_F = 70°C$.

extracellular matrix [25]. From this point of view, the microarchitecture of the scaffold must provide an ideal environment of physical confinement for cells and tissues, but also an adequate nutrient supply and mechanical function [3,6,10,25].

In the past few years, GF-based techniques have emerged as very promising tools for the design of porous synthetic scaffolds with finely controlled biochemical and biophysical properties; this approach also avoids the use of organic solvents potentially harmful to cells and tissues [26,27]. In fact, using this solvent-free technique, it has been possible to prepare scaffolds with biomimetic porous structures and functional fillers [28,29], as well as scaffolds containing preincorporated cells and possessing the ability to deliver active growth factors in a controlled fashion [30–32].

We recently reported a new technique for the design and preparation of PCL scaffold with a multiscaled microarchitecture and high degree of pore interconnection, by the combined GF–PE technique [19]. In the current study, we

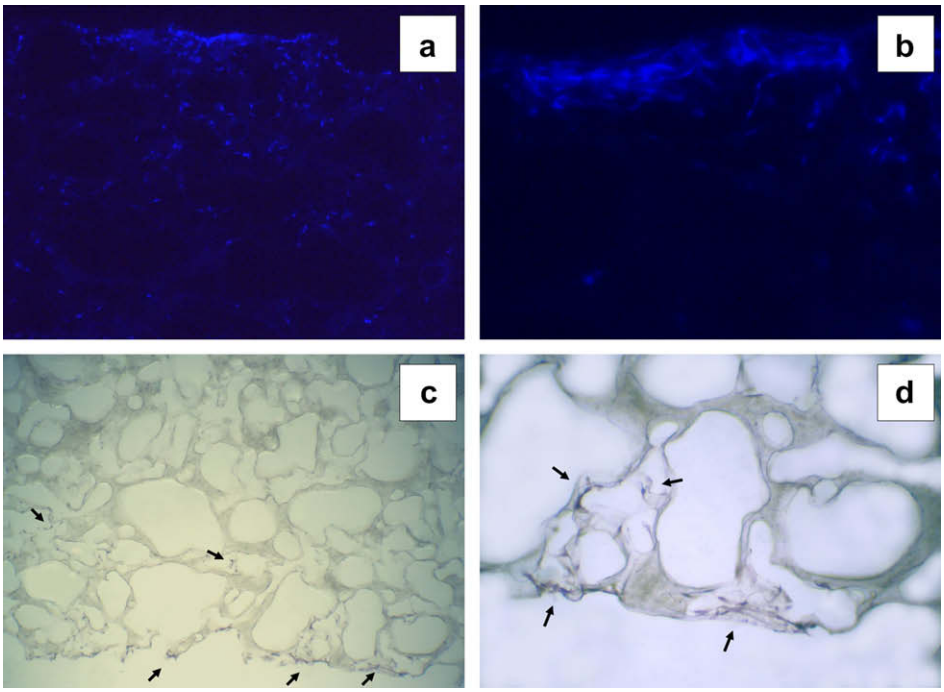

Fig. 8. (a, b) Fluorescence microscope and (c, d) histology images of the cross sections of the cell-scaffold constructs at 1 day. Figure (a) objective 4x, figure (b) objective 10x.

evaluated the ability of this scaffold to satisfy key microstructural and biological tissue engineering scaffold requirements. In particular, this study was mostly devoted to assessing the possibility of promoting and guiding hMSC proliferation and 3-D colonization by appropriately designing the topological characteristics of the scaffold.

As reported in Table 1, the μ-bimodal PCL scaffold prepared was characterized by an overall porosity of 62%, uniformly distributed between macroporosity (44%) and microporosity (56%). These microstructural parameters have been designed by selecting a 3/2 (w/w) PLC/TG and optimizing the GF processing conditions. Although higher TG concentration is expected to positively affect cell behaviour, for 'soft' biomaterials such as the PCL selected in this work, a lower templating concentration and, therefore a low overall porosity amount, may avoid reducing the mechanical function of the scaffold [33]. From this point of view, the selection of a continuous templating, instead of the commonly used particulate templating (e.g. NaCl) [27], may be also preferable because it allows the overall porosity of the scaffold to be reduced, without compromising the interconnection among the pores (Fig. 1a and c) [19,34]. Consequently, the final μ-bimodal PCL scaffold prepared was characterized by high interconnectivity and good mechanical responses, as evidenced by the SEM micrograph of Fig. 1c and by the average elastic compression modulus and compression yield strength values reported in Table 1.

The cell–scaffold interaction study was performed by using bone-marrow-derived hMSCs, seeded on the surface of the scaffold and cultured in vitro, for 21 days under static conditions. The results of the Alamar Blue assay demonstrated the ability of the scaffold to promote hMSC adhesion and proliferation. Indeed, the number of cells progressively increased up to 3 times, from day 1 to day 21 (Fig. 2). The number of cells reported at day 1 (~60,000) was less than the number of cells inoculated at the start (~400,000), indicating that most of the hMSCs seeded on the scaffold surface penetrated the inner region of the scaffold, even early in the experiment. This assumption is corroborated by the CLSM analysis reported in Fig. 5 and, by the fact that the Alamar Blue assay may fail to count cells seeding inside the 3-D scaffold [33].

The SEM and fluorescence microscopy images reported in Figs. 3 and 4, respectively, confirmed the Alamar Blue results, showing the adhesion and proliferation of the hMSCs over all the culture time investigated. In particular, at 21 days after seeding, the cell proliferation resulted in the formation of a dense cell sheet on the surface of the scaffold (Figs. 3f and 4).

These results are consistent with those recently reported in the literature, which showed the ability of PCL scaffolds to support hMSC adhesion and proliferation in vitro [17,35–37]. However, our scaffold presented an enhanced 3-D cell distribution and colonization/proliferation. In particular, compared to the salt leaching-based PCL scaffolds [36], we observed enhanced hMSC proliferation under the same culture conditions, while proliferation index comparable to our results has been achieved for 2-D cell-culture on PCL film [37]. The ability of a scaffold to support and guide the regeneration process of new tissue is strongly dependent on the combination of cells, chemistry and its

microarchitectural properties. Therefore, although it is difficult to discriminate between the effects of the different parameters on the cell–scaffold interaction, we postulate that the enhancement reported in this work can be partly ascribed to the TG used as templating. Indeed, a thin coating of this polymeric material may be still present into the microstructure of the scaffold, even after the removal of the TG from the foamed blend.

Cell colonization in 3-D is essential in tissue engineering scaffold-based strategies for the regeneration of functional biological tissues [38]. Therefore, the optimization of cell distribution in 3-D represent one of the most critical aspects of scaffold design. Indeed, a large number of studies have shown that, without a dynamic seeding strategy, cell adhesion and colonization preferentially occurred on the scaffold surface, while very poor cell seeding efficiency may be achieved in the inner region of the scaffold [12,17,38].

The ability of the μ-bimodal PCL scaffold prepared to promote 3-D cell colonization under static seeding conditions was supported by the fluorescence microscopy images and histological analysis of the cross-sections of the cell–scaffold constructs, which also evidenced the consistent and selective cell infiltration into the macroporosity, compared to the microporosity (Figs. 5 and 6). This effect may be explained by considering that, during seeding, the cell suspension preferentially perfused through the macroporosity. Consequently, depletion of hMSC adhesion and colonization into the microporosity occurred (Figs. 5 and 6). Indeed, the topological characteristic of the macroporosity, characterized by a microtubular architecture with reduced tortuosity and enhanced permeability if compared to the microporosity (see Fig. 1), may promote cell seeding efficiency and fluid diffusion, even though these characteristics are hindered by the hydrophobic nature of the PCL [39]. The analysis of the cross-sections of the cell–scaffold constructs also showed that, over the culture time, the cells within the scaffold remained viable, as suggested by the shape of their nuclei (see Fig. 5e and f), and then these cells proliferated and stretched, creating bridges between the opposite macroporosity walls (Figs. 3g and 6c–f).

The enhancement of hMSC adhesion and 3-D colonization into the μ-bimodal PCL scaffolds was also supported by the results of the cell–scaffold interaction study performed on monomodal PCL scaffolds. In particular, the monomodal scaffolds selected for the comparative study were prepared by the same combined GF–PE technique and performing the foaming process at $T_F = 70$ °C. Indeed, by choosing a T_F higher than the PCL melt temperature it was possible to prepare scaffolds with a comparable value of overall porosity (61%) but characterized by a monomodal pore size distribution (see Fig. 7). As evidenced in Fig. 8, and unlike the cell distribution observed into the μ-bimodal PCL scaffolds (see Figs. 5a and 6a) when seeded on the monomodals scaffolds, the hMSCs preferentially adhered to the scaffold surface, while depleted 3-D cell colonization was observed in the inner region of the porous structure (Fig. 8a and c). Furthermore, the difficulty cell suspensions have in perfusing into the interior of the scaffold was also responsible of the heterogeneous distribution of cells on the scaffold surface, as reported in Fig. 8b and d.

Similar results have been reported by Silva et al. [40], who showed that an anisotropic scaffold microarchitecture, characterized by aligned channels incorporated into an ordered porous structure, may improve fluid transport and cell-tissue infiltration into the interior of a construct. This microarchitecture has been obtained by the combination of GF and reverse templating techniques, using metallic templating needles to create an elongated and oriented porosity. By considering our results and those reported in Ref. [40] it is possible to see that an optimal combination of pore size and shape is essential to promote and guide the colonization of cells in 3-D. In particular, the topological properties of the GF pores may have a strong influence on cell adhesion and colonization. Indeed, the low size of the GF pores of the μ-bimodal PCL scaffolds prepared in this study, coupled with the hydrophobic nature of the polymeric matrix, may hinder hMSC colonization into the microporosity. Therefore, the cells preferentially invade the macroporosity. This aspect may be very important for in vitro scaffold-based tissue engineering strategies. Indeed, one of the most important limitations of tissue engineering scaffold is that cell proliferation and extracellular matrix deposition may progressively occlude the entire porosity of the scaffold and, consequently reduce nutrient delivery to, and metabolic waste removal from, the interior of the construct [10]. Therefore, even if a large number of studies have pointed out the importance of an uniform cell infiltration in 3-D, the presence of a microporosity network not accessible for cells should be very important because of the possibility of ensuring the transport of fluids necessary for cell biosynthesis.

Although this cell–scaffold interaction study has demonstrated the ability of the μ-bimodal PCL scaffold prepared herein to support and guide hMSC adhesion, proliferation and 3-D colonization, more detailed in vitro and in vivo studies will be necessary. In particular, these studies will be performed with the aim of assessing the efficacy of the multiscaled microarchitecture designed to support cell proliferation and the formation new tissue over longer culture times.

5. Conclusions

In this study we characterized the ability of novel μ-bimodal porous PCL scaffold to promote and guide hMSC adhesion, proliferation and 3-D colonization.

The selection of a continuous templating agent and the optimization of the GF parameters allowed the preparation of PCL scaffold with a multiscaled microarchitecture and functional mechanical properties. Furthermore, the results of the cell–scaffold interaction study demonstrated that high cell seeding efficiency and 3-D colonization may be achieved by fine tuning the topological characteristics

of the scaffold. In particular, the μ-bimodal PCL scaffold prepared promoted selective 3-D hMSC colonization into the macroporosity, and consequently ensured the presence of a separate porous network for fluid transport.

All these results demonstrate the importance of scaffold design to guide the regeneration process of new tissue starting from the cell/material construct, and indicate possible future directions to overcome the diffusion constraints that limit the great potential of scaffold-based strategies.

Acknowledgments

The authors thank Diego Gerbasio for helping out with the histological characterization and Prof. De Berardinis for the γ-sterilization.

References

[1] Langer R, Vacanti JP. Tissue engineering. Science 1993;260(5110):920–6.
[2] Griffith LG, Naughton G. Tissue engineering – current challenges and expanding opportunities. Science 2002;295(5557):1009–14.
[3] Kim B, Mooney DJ. Development of biocompatible synthetic extracellular matrices for tissue engineering. Tibtech 1998;16(5):224–30.
[4] Chen G, Ushida T, Tateishi T. Scaffold design for tissue engineering. Macromol Biosci 2002;2(2):67–77.
[5] Hollister SJ. Porous scaffold design for tissue engineering. Nat Mater 2005;4(7):518–24.
[6] Yang S, Leong K, Du Z, Chua C. The design of scaffolds for use in tissue engineering. Part I. Traditional factors. Tissue Eng 2001;7(6):679–89.
[7] Karageorgiou V, Kaplan D. Porosity of 3D biomaterial scaffolds and osteogenesis. Biomaterials 2005;26(27):5474–91.
[8] Zeltinger J, Sherwood JK, Graham DA, Mueller R, Griffith LG. Effect of pore size and void fraction on cellular adhesion, proliferation, and matrix deposition. Tissue Eng 2001;7(5):557–72.
[9] Moore MJ, Jabbari E, Ritman EL, Lu L, Currier BL, Windebank AJ, et al. Quantitative analysis of interconnectivity of porous biodegradable scaffolds with micro-computed tomography. J Biomed Mater Res 2004;71A(2):258–67.
[10] Karande TS, Ong JL, Agrawal CM. Diffusion in musculoskeletal tissue engineering scaffolds: design issues related to porosity, permeability, architecture, and nutrient mixing. Ann Biomed Eng 2004;32(12):1728–43.
[11] Glowacky J, Mizuno S, Greenberger JS. Perfusion enhances functions of bone marrow stromal cells in three-dimensional culture. Cell Transplant 1998;7(3):319–26.
[12] Goldstein AS, Juarez TM, Helmke CD, Gustin MC, Mikos AG. Effect of convection on osteoblastic cell growth and function in biodegradable polymer foam scaffolds. Biomaterials 2001;22(11):1279–88.
[13] Wendt D, Marsano A, Jakob M, Heberer M, Martin I. Oscillating perfusion of cell suspensions through three-dimensional scaffolds enhances cell seeding efficiency and uniformity. Biotech Bioeng 2003;84(2):205–14.
[14] Mygind T, Stiehler M, Baatrup A, Li H, Zou X, Flyvbjerg A, et al. Mesenchymal stem cell ingrowth and differentiation on coralline hydroxyapatite scaffolds. Biomaterials 2007;28(6):1036–47.
[15] Serrano MC, Pagani R, Vallet-Regí M, Peña J, Rámila A, Izquierdo I, et al. In vitro biocompatibility assessment of poly(ε-caprolactone) films using L929 mouse fibroblasts. Biomaterials 2004;25(25):5603–11.
[16] Sun H, Mei L, Song C, Cui X, Wang P. The in vivo degradation, absorption and excretion of PCL-based implant. Biomaterials 2006;27(9):1735–40.
[17] Savarino L, Baldini N, Greco M, Capitani O, Pinna S, Valentini S, et al. The performance of poly-ε-caprolactone scaffolds in a rabbit femur model with and without autologous stromal cells and BMP4. Biomaterials 2007;28(20):3101–9.
[18] Tay BY, Zhang SX, Myint MH, Ng FL, Chandrasekaran M, Tan LKA. Processing of polycaprolactone porous structure for scaffold development. J Mater Process Tech 2007;182(1–3):117–21.
[19] Salerno A, Oliviero M, Di Maio E, Iannace S, Netti PA. Design and preparation of μ-bimodal porous scaffold for tissue engineering. J Appl Polym Sci 2007;106(5):3335–42.
[20] Ho ST, Hutmacher DW. A comparison of micro CT with other techniques used in the characterization of scaffolds. Biomaterials 2006;27(8):1362–76.
[21] Whitaker S. Advances in theory of fluid motion in porous media. Ind Eng Chem 1969;61(12):14–28.
[22] Kwak KD, Okada M, Chiba T, Nose T. Electron-microscopic study of the coexistence curve of polystyrene/poly(2-chlorostyrene) blends. Macromolecules 1992;25(26):7204–7.
[23] Gibson LJ, Ashby MF. The mechanics of foams: basic results. In: Clarke DR, Suresh S, Ward IM, editors. Cellular solids. Cambridge: 1997. p. 175–217.
[24] Gloeckner H, Jonuleit T, Lemke H. Monitoring of cell viability and cell growth in a hollow-fiber bioreactor by use of the dye Alamar Blue. J Immunol Methods 2001;252(1–2):131–8.
[25] Causa F, Netti PA, Ambrosio L. A multi-functional scaffold for tissue regeneration: the need to engineer a tissue analogue. Biomaterials 2007;28(34):5093–9.
[26] Mooney DJ, Baldwin DF, Suh NP, Vacanti JP, Langer R. Novel approach to fabricate porous sponges of poly(D,L-lactic-co-glycolic acid) without the use of organic solvents. Biomaterials 1996;17(14):1417–22.
[27] Harris DL, Kim B, Mooney DJ. Open pore biodegradable matrices formed with gas foaming. J Biomed Mater Res 1998;42(3):396–402.
[28] Mathieu LM, Mueller TL, Bourban P, Pioletti DP, Muëller R, Månson JE. Architecture and properties of anisotropic polymer composite scaffolds for bone tissue engineering. Biomaterials 2006;27(6):905–16.
[29] Mathieu LM, Montjovent MO, Bourban P, Pioletti DP, Månson JE. Bioresorbable composites prepared by supercritical fluid foaming. J Biomed Mater Res 2005;75(1):89–97.
[30] Ginty PJ, Howard D, Upton CE, Barry JJA, Rose FRAJ, Shakesheff KM, et al. A supercritical CO_2 injection system for the production of polymer/mammalian cell composites. J Supercrit Fluid 2008;43(3):535–41.
[31] Richardson TP, Peters MC, Ennett AB, Mooney DJ. Polymeric system for dual growth factor delivery. Nat Biotech 2001;19(11):1029–34.
[32] Kanczler JM, Ginty PJ, Barry JJA, Clarke NMP, Howdle SM, Shakesheff KM, et al. The effect of mesenchymal populations and vascular endothelial growth factor delivered from biodegradable polymer scaffolds on bone formation. Biomaterials 2008;29(12):1892–900.
[33] Shor L, Güçeri S, Wen X, Gandhi M, Sun W. Fabrication of three-dimensional polycaprolactone/hydroxyapatite tissue scaffolds and osteoblast-scaffold interactions in vitro. Biomaterials 2007;28(35):5291–7.
[34] Sarazin P, Roy X, Favis BD. Controlled preparation and properties of porous poly(L-lactide) obtained from a co-continuous blend of two biodegradable polymers. Biomaterials 2004;25(28):5965–78.
[35] Marletta G, Ciapetti G, Satriano C, Perut F, Salerno M, Baldini N. Improved osteogenic differentiation of human marrow stromal cells cultured on ion-induced chemically structured poly-ε caprolactone. Biomaterials 2007;28(6):1132–40.
[36] Guarino V, Causa F, Netti PA, Ciapetti G, Pagani S, Martini D, et al. The role of hydroxyapatite as solid signal on performance of PCL porous scaffolds for bone tissue regeneration. J Biomed Mater Res B Appl Biomater 2008;86B(2):548–57.

[37] Chastain SR, Kundu AK, Dhar S, Calvert JW, Putnam AJ. Adhesion of mesenchymal stem cells to polymer scaffolds occurs via distinct ECM ligands and controls their osteogenic differentiation. J Biomed Mater Res 2006;78A(1):73–85.

[38] Alvarez-Barreto JF, Linehan SM, Shambaugh RL, Sikavitsas VI. Flow perfusion improves seeding of tissue engineering scaffolds with different architectures. Ann Biomed Eng 2007;35(3):429–42.

[39] Vidaurre A, Cortázar IC, Ribelles JLG. Polymeric scaffolds with a double pore structure. J Non-Cryst Solids 2007;353(11–12): 1095–100.

[40] Silva MMCG, Cyster LA, Barry JJA, Yang XB, Oreffo ROC, Grant DM, et al. The effect of anisotropic architecture on cell and tissue infiltration into tissue engineering scaffolds. Biomaterials 2006;27(35):5909–17.